Electronic Supplementary Information (ESI)

Self-Powered Flexible Fe-doped RGO/PVDF Nanocomposite: An Excellent Material for Piezoelectric Energy Harvester

Sumanta Kumar Karan[1], Dipankar Mandal[2], Bhanu Bhusan Khatua[1,*]

[1]Materials Science Centre, Indian Institute of Technology Kharagpur, Kharagpur 721302, India.

[2]Organic Nano-Piezoelectric Device Laboratory, Department of Physics, Jadavpur University, Kolkata 700032, India.

*Corresponding Author: Dr. B. B. Khatua (E-mail: khatuabb@matsc.iitkgp.ernet.in)

Materials Science Centre, Indian Institute of Technology Kharagpur, Kharagpur-721302, India

Tel: 91-3222-283982.

S1. Experimental

S1.1. Synthesis of graphene oxide (GO)

GO was synthesized by oxidizing of natural graphite powder according to modified Hummer method.[1] In brief, 4 g graphite powder and 2 g $NaNO_3$ were well mixed, and then ≈ 92 ml concentrated H_2SO_4 (98%) was added to the mixture in an ice bath. After that, mixture was stirring uniformly followed by sonication for 1 h. Then, $KMnO_4$ (12 g) was slowly added to the mixture under stirring condition at low temperature (below 20 ºC). The solution mixture was then transferred to an ice cool water bath and stirring for 24 h at room temperature. Furthermore, distilled water (190 ml) was added slowly to the mixture by controlling temperature. Again, ice-cold water (400 ml) was added to the mixture with constant stirring. Finally, 30% H_2O_2 was added drop wise until the color of the reaction mixture transferred to bright yellow and continued the stirring for another 1h. The mixture was left for overnight. After that, the reaction mixture was filtered, washed by centrifugation for several times using 5% HCl solution and distilled until the solution became neutral. Finally, the oxidized graphite was washed several times with ethanol and dried in vacuum oven at 40 ºC for 3 days to obtain the ultimate product.

S1.2. Preparation of RGO and Fe-doped RGO

RGO was synthesized by the reduction of GO in the presence of iron (Fe) powder and HCl.[2] At first, as prepared GO (0.5 mg/ml) was dispersed in distilled water through ultra-sonication (OSCAR Model PR-250; Ultrasonic Power, Frequency 25 kHz, diameter of Probe Tip is 6 mm). Then, water dispersed Fe powder (5 g) was added to the suspended GO and continued ultrasonication for 90 m. After that, 100 ml of HCl solution (35%) was added in the GO mixture and sonicated for another 90 min. The resulting solution was filtered and washed with distilled water (to maintain $p^H \approx 7$) and ethanol for several times. Finally, the obtained solid was dried in

vacuum oven at 60 ºC for 24 h. During the reduction process, some Fe particles have been incorporated into the surface of RGOs, as confirmed by EDX (Fig. S5 and Fig. S6) and XPS analysis. We assume that Fe not only reduced the GO to RGO, but also remain present in RGO as a dopant. This Fe was present in the RGOs as oxide of Fe and/or pure Fe metal (confirmed by XPS study). Mixture of Fe and Fe-oxide containing RGO is referred as Fe doped RGO (Fe-RGO) throughout the description.

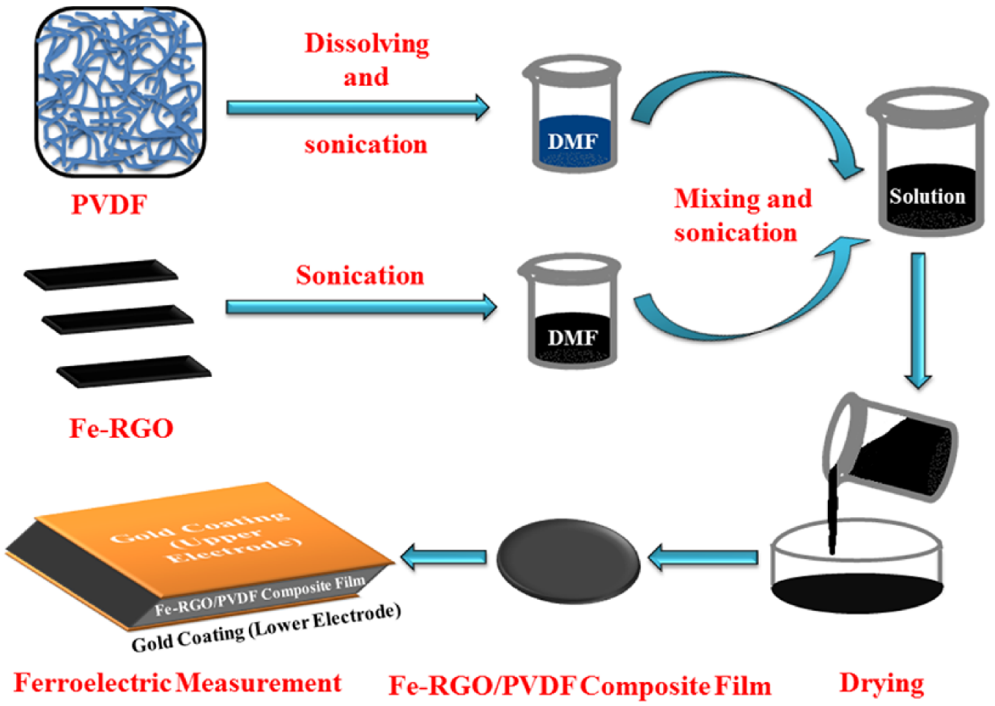

Fig. S1 Schematic diagram of the fabrication procedure of Fe-RGO/PVDF nanocomposite film

S2. Results and discussion

S2.1. Confirmation of GO and Fe-RGO

XRD analysis was carried out for the confirmation of GO and Fe-RGO formation, as shown in Fig. S2(A). An intense peak is observed at $2\theta \approx 10^{\circ}$ and a small broadened peak at $2\theta \approx 23.4^{\circ}$ suggesting the formation of GO and Fe-RGO, respectively.[2] It is noteworthy; the presence of any characteristic peak for Fe is not appeared, that could be due to the presence of very small amount

of Fe into RGOs (≈ 1 atomic wt%, confirmed from XPS study). The presence of Fe in the RGO, as well as, in the nanocomposite was confirmed by XPS and EDX analysis. We assume that Fe not only reduced the GO to RGO, but also remain present in RGO as a dopant. This Fe was present in the RGOs as oxide of Fe and/or pure Fe metal, confirmed by XPS study (Fig. S3). Mixture of Fe and Fe-oxide containing RGO is referred as Fe doped RGO (Fe-RGO) throughout the description. Presence of sheet like structure of in RGO as well as in the nanocomposite was clearly confirmed from FESEM and TEM studies (Fig. S5). The presence of Fe and the oxygen content in RGO was greatly reduced compared to GO after reduction, as confirmed from EDX analysis of Fe-RGO (Fig. S6 and Fig. S7).

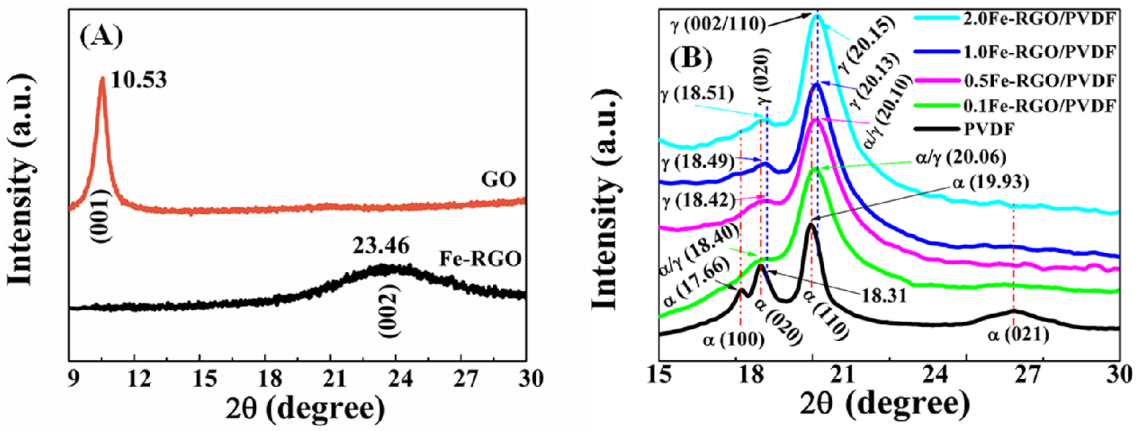

Fig. S2 X-ray diffraction patterns of (A) GO and RGO, and (B) pure PVDF and Fe-RGO/PVDF nanocomposite[3] at different Fe-RGO loading.

The XPS analysis is the most suitable experiment for the elemental analysis and their ratios of the materials. Fig. S3 shows the XPS analysis of GO and Fe-RGO and the C1s and O1s spectra are appeared at 284 and 533 eV, respectively. As observed, the intensity of O1s is reduced significantly for RGO compared to the GO after the chemical reduction. The increased C/O ratio from GO (2.0) to RGO (6.9) is the indication of the reduction of the GO. From XPS

survey scans spectra (Fig. S3(A)) of Fe-RGO and GO, the materials are approximately pure with the presence of small amount of Fe and/iron oxides particles. Only carbon, oxygen and Fe are present in the materials. From this analysis, five different peaks are appeared at 283.7, 285, 286.2, 287.7 and 288 eV which are the corresponding values of the sp^2C, sp^3C, –C–O, –C=O and –COO– groups, respectively.[2] After the reduction of GO, the intensities of C1s spectra is drastically increased in Fe-RGO compared to the GO. The sp^3 C peak intensity decreases and sp^2 C peak intensity increases which are shown in Fig. S3(C). So, it can unambiguously be concluded that, the oxygen functionality are reduced and most of the conjugated type RGO network has been restored after the reduction of GO.

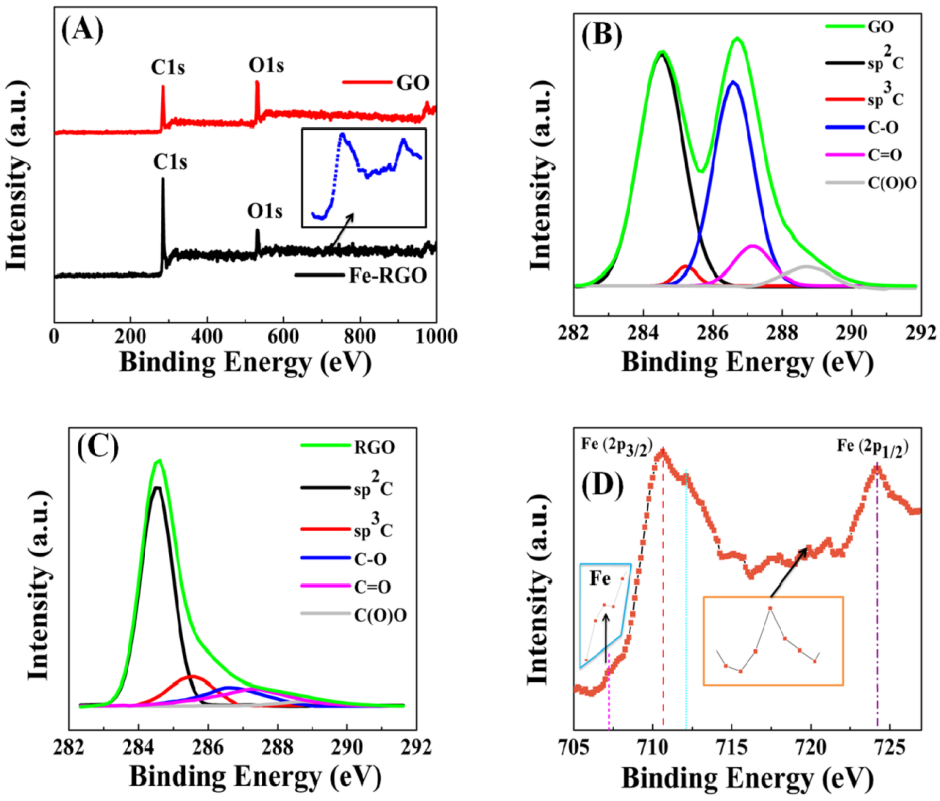

Fig. S3 XPS survey spectra (A) of GO and Fe-RGO (Fe present in Fe-RGOs shown by zoom in inset) with high resolution (deconvoluted) C1s spectra of (B) GO and (C) Fe-RGO and energy

spectrum of (D) Fe_{2p} with showing different oxidation state and satellite formation (showing in inset).

Fig. S3(D) shows the existence of iron intense peak in Fe-RGO. During the reduction, Fe/Fe-oxides particles may be encapsulated in RGO layers. Fig. S3(D) shows the narrow XPS spectrum of Fe_{2p} which reveals that Fe can exists in the different oxidized forms. The intense peaks are observed at 710.6 and 724.1 eV assigned to Fe $_{2p3/2}$ and Fe $_{2p1/2}$, respectively. These two peaks are probably due to the presence of different oxide of Fe particles during the reduction. It is notified that, charge transfer satellite of Fe 2p3/2 at about 719.9 eV is observed with the formation of different valence of Fe (II and III) in the Fe-RGOs.[4–6] In addition, there is another less intense peak (712.1 eV) present in Fe-RGO assigned to Fe (III). However it is difficult to identify properly which oxide forms are present in the materials. Though this study cleared about the existence of Fe and its oxides form in the Fe-RGOs, which is present in the nanocomposites affecting many properties.

Raman spectroscopy is strongly depended on the materials electronic structure. To characterize the GO and Fe-RGO from Raman spectroscopy, the two main fundamental vibrations parameter are considered. One is D vibration mode, which is arising due to the breathing mode of k-point photons of A_{1g} symmetry (generally shown at 1350 cm^{-1}) and another is G mode which is developed for the E_{2g} phonon of first order scattering of sp^2 C atoms (generally shown at 1575 cm^{-1}).[7]

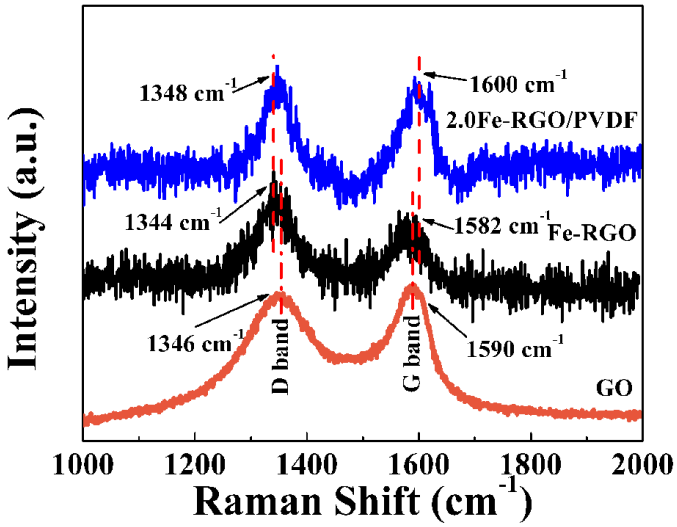

Fig. S4 Raman spectra of GO, Fe-RGO and 2.0Fe-RGO/PVDF nanocomposite.

For GO, G band appeared at 1590 cm^{-1} which is little broadened (Fig. S4) and shifted due to the presence of isolated double bonds that resonating with higher frequency than the G-band of graphite[8] and the D band was observed at 1346 cm^{-1}. This D band becomes prominent which indicated the decrease in size of the in plane sp^2 domains, probably for the extensive oxidation.[9] In the case of Fe-RGO, the G-band and D-band are appeared at 1582 cm^{-1} and 1344 cm^{-1}, respectively (Fig. S4), due to recovery of the hexagonal network of carbon atoms with defects. After reduction of GO, the intensity ratio of D band to G band (I_D/I_G) was marginally increased (from 0.94 to 1.10) due to the unrepaired defect backbone of RGO which remain after the removal of oxygen functionality.[2] This slight increasing value of I_D/I_G ratio suggested that the average size of the sp^2 domain decreases with the reduction of GO. This phenomenon may happen due to the development of numerous new graphitic domains which are small in size compared to that of RGO.[10] The reduction of GO to RGO was also confirmed from XPS analysis.

As shown in Fig. S5(A) and Fig. S5(B), the sheet like structure of Fe-RGO is observed which is composed of multilayer's Fe-RGOs due to the re-stacking of the layer during the reduction process. The π–π interaction among the RGO nanosheets may play to re-stack the layers. Fig. S5(B) clearly shows the re-stacking of the layers. In addition, the selected area electron diffraction (SAED) pattern of Fe-RGO nanosheet has been studied, as shown in inset of Fig.S5(B) which supported the multilayer structure and crystalline nature of Fe-RGO. EDX analysis of the Fe-RGO and nanocomposite also confirmed the presence of Fe in both the materials, respectively, which can affect many properties, as shown in Fig. S6 and Fig. S7.

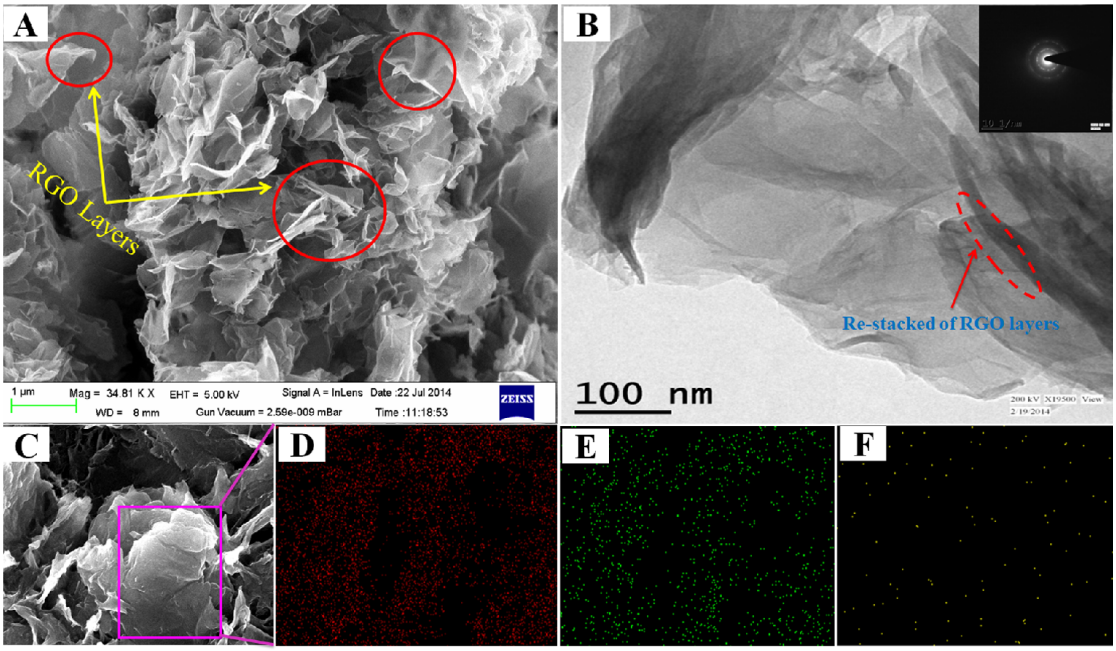

Fig. S5 FESEM and HRTEM images of (A, B) Fe-RGO and X-ray mapping of Fe-RGO (C) for C atom (D), O atom (E) and Fe particles (F), respectively. SAED patterns of Fe-RGO shows the crystalline nature of Fe-RGOs in inset (B).

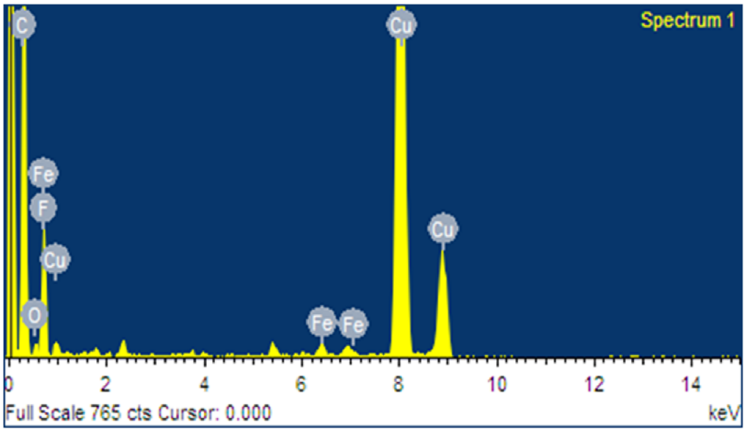

Fig. S6 EDX spectrum of Fe-RGO/PVDF nanocomposites under HR-TEM study. It exhibits the presence of carbon (C), oxygen (O) fluoride (F) and Fe atom in the nanocomposite.

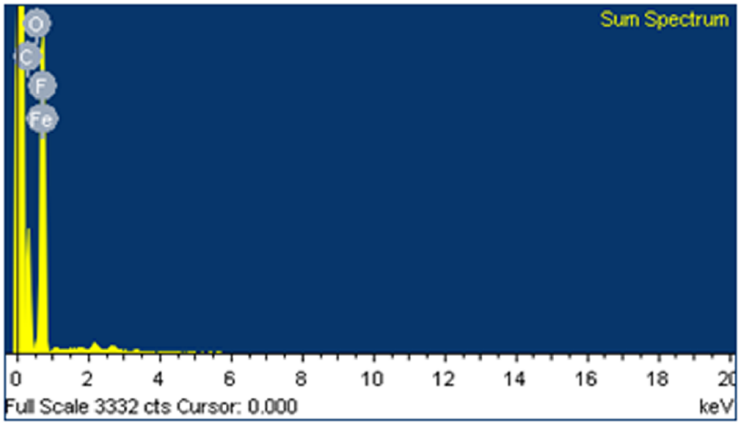

Fig. S7 EDX spectrum of Fe-RGO/PVDF nanocomposites from FESEM study. It exhibits the presence of carbon (C), oxygen (O) and fluoride (F) signal arising from composites and small peak appear of Fe atom.

S2.2. Electrical conductivity

The DC electrical conductivity (σ_{DC}) (in term of surface conductivity and not the bulk conductivity) of the PVDF and Fe-RGO/PVDF nanocomposite at different loadings (0.1, 0.5, 1.0 and 2.0 wt %) of Fe-RGO was measured at room temperature. As observed, (Fig. S8), the σ_{DC} value of the nanocomposite gradually increases with increasing of filler content. At 0.5 wt% loading, the electrical conductivity suddenly reaches to $\approx 5.93\times10^{-6}$ S.cm^{-1}. On further addition of Fe-RGO, the electrical conductivity was gradually increased. The maximum surface

conductivity of the Fe-RGO/PVDF nanocomposite film reached up to ≈ 3.30×10^{-3} S.cm^{-1} at 2.0 wt% filler loading. The presence of Fe-RGO sheets in the nanocomposite forms a π-π interaction between the base polymer and Fe-RGO throughout the matrix. This affinity plays a key role to increase the conductivity of the nanocomposite through the formation of conductive network structure of Fe-RGO in the nanocomposite. The percolation threshold (p_c) of the nanocomposite was found in between 0.1 and 0.5 wt% filler loading.

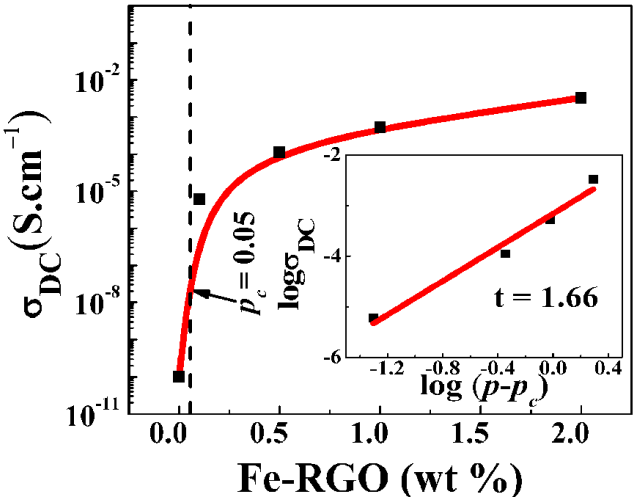

Fig. S8 DC electrical conductivity (surface conductivity) of Fe-RGO/PVDF nanocomposite films at different Fe-RGO contents. Inset: log-log plot for σ_{DC} versus (p-p_c) for the same nanocomposite. The straight line in the inset is a least squares fit to the data, showing the best fit values p_c = 0.05% and t = 1.66.

The p_c of the Fe-RGO/PVDF nanocomposite can be estimated with the help of the following power law equation.[11]

$$\sigma_{DC} \propto (p - p_c)^t \qquad for \qquad p > p_c \qquad (1)$$

Where, σ_{DC} is the DC conductivity of the nanocomposite, p is weight concentration of nanofiller and t is the critical exponent.

Using the above equation 1, a linear plot of conductivity vs. $log\ (p - p_c)$ has been achieved, as shown in inset of Fig. S8. From this plot, p_c value has been calculated and the measured value was 0.05 wt% for the nanocomposite and the critical exponent (t) was measured using the slope which was found to be $t = 1.66$ with the standard deviation of $\pm$ 0.190. The critical exponent (t) value of the nanocomposite is close to the universal value of 3D percolation network.[12] The percolation threshold indicated the homogeneous dispersion of Fe-RGO throughout the nanocomposite and formed a conducting network structure which help to reduce the percolation threshold and increased the surface conductivity at such low filler loading. The conducting nature (insulating and conducting) of the Fe-RGO/PVDF nanocomposite film along thickness direction (top and bottom), on the surface and among the edges are shown by schematically and optically (real images of resistance measurement) in Fig. S9 and Fig. S10, respectively. The film is insulating in nature between the edges before silver coating but is conducting in nature after silver pasting. This is because of connection between the surface and the edges through silver coating. Actually, the surface of the film is conducting (not the bulk conductivity) in nature but it is insulating in nature along thickness (top to bottom) direction.

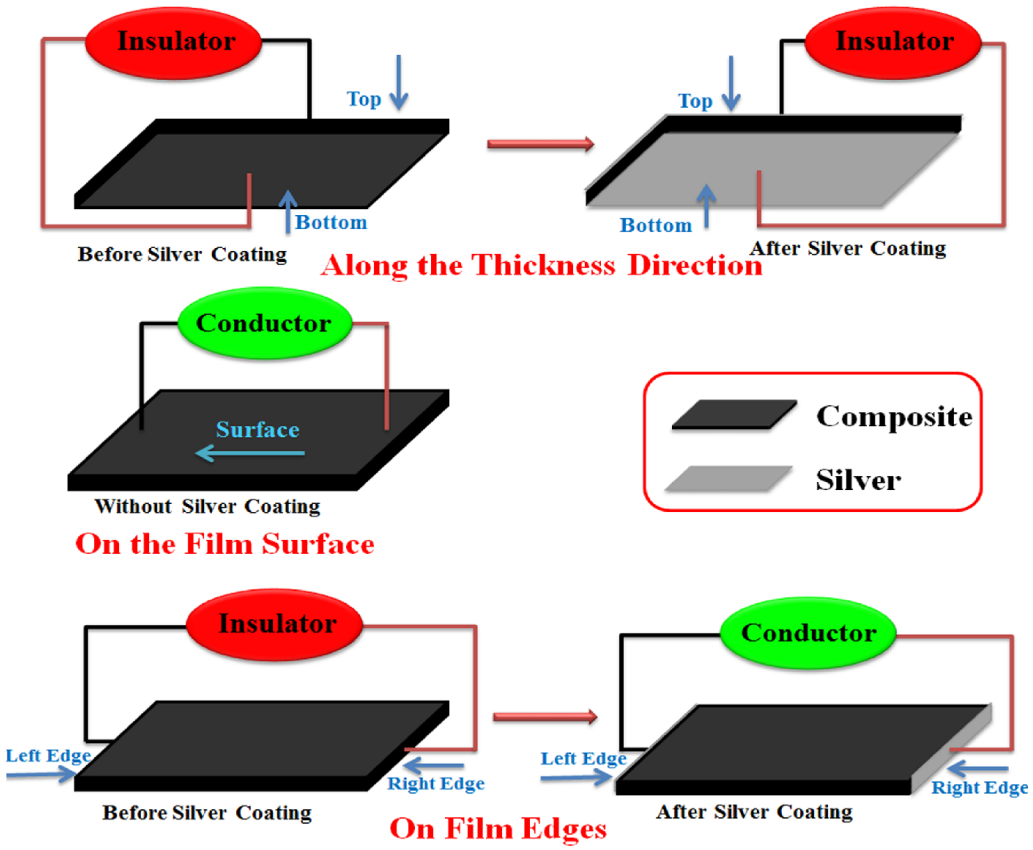

Fig. S9 Schematic diagram represent the insulating and conducting nature of Fe-RGO/PVDF nanocomposite film in different direction. Along the thickness direction (between top and bottom electrode) it is insulating nature both before and after the silver coating (top and bottom surface). The surface of the film is always in conducting in nature. Between the two edges, the film is insulating and conducting in nature before and after the silver coating.

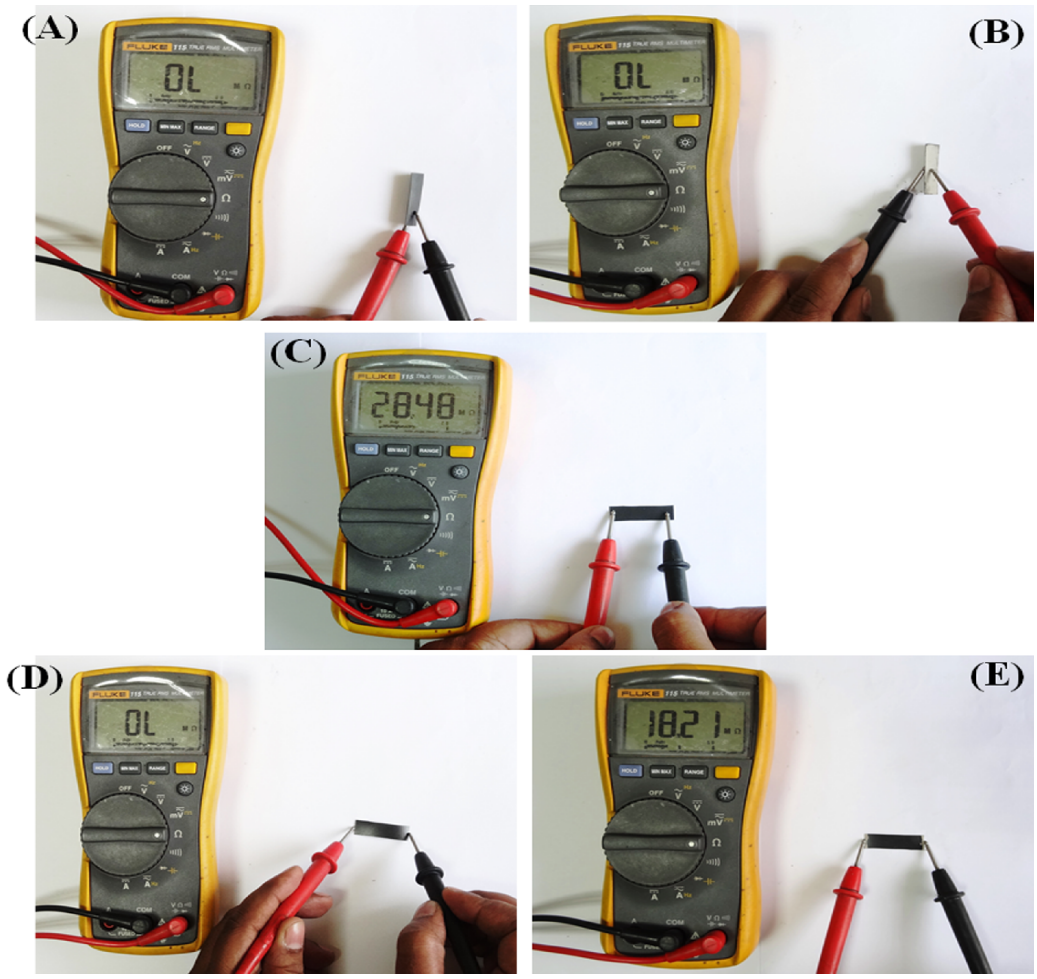

Fig. S10 The digital images of resistance measurement of Fe-RGO/PVDF nanocomposite film. Along the thickness direction (between top and bottom electrode), it illustrating the insulating in nature both before (A) and after (B) the silver coating (top and bottom surface). The surface of the film shows in conducting in nature (C). The film is also insulating and conducting in nature between the two edges both before (D) and after (E) the silver coating, respectively.

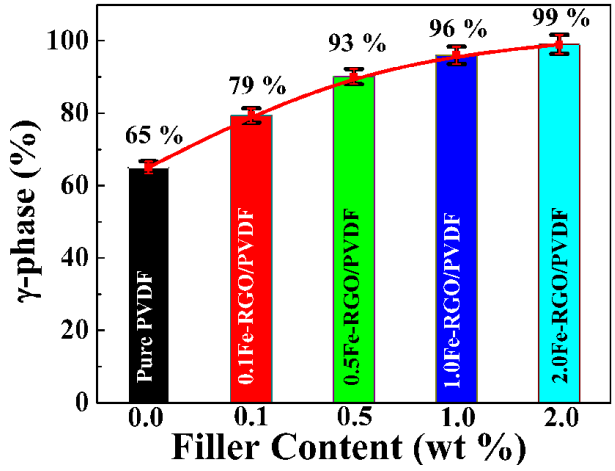

Fig. S11 The relative proportion of γ-phase (%) formation in PVDF and Fe-RGO/PVDF nanocomposite at different filler concentration.

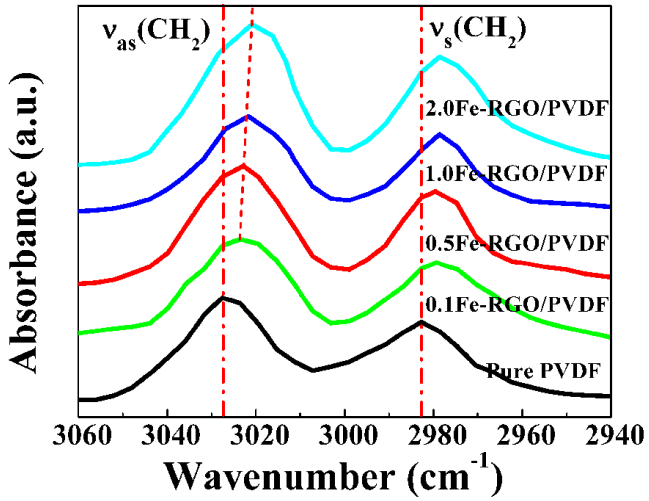

Fig. S12 FT-IR spectra in the region of 3060-2940 cm^{-1} of pure PVDF and Fe-RGO/PVDF nanocomposites at different filler loading.

S2.3. Applied pressure (σ) calculation and current density evaluation

Human finger imparting pressure is calculated on the basis of physical model combining the gravity and pulse term.[13] During the falling an object (human figure in our work) on the film surface, there exist two processes: 1) initially touch the surface of the film, and 2) then

completely acting on the film. In the first process, the descending velocity of the object increases to a maximum value and in second process it decreases to zero. Hence, based on the kinetic energy and momentum theorem, we have the following equations:

$$m.g.h = \frac{1}{2}mv^2 \quad (2)$$

$$(F - m.g).\Delta t = m.v \quad (3)$$

$$\sigma = \frac{F}{S} \quad (4)$$

Where, m is the mass of the object, h is the height from where it is fall, v is the maximum falling velocity, σ is the applied pressure or applied stress, F is the contact force, S is the effective contact area and Δt is the time span during the second process.

Here, S= 520 mm^2 is the approximate active area (effective area) of the electrode (area under the external pressure), m= 0.41 kg is measured using laboratory balance, Δt = 0.20 sec is the estimated average time difference between the two consecutive voltage peak, h = 0.06 m is the approximate height and g = 9.80 N/kg.

Therefore, these values calculate the input force, F ≈ 6.23 N, which gives the approximate contact pressure in the order of σ ≈ 12.00 kPa.

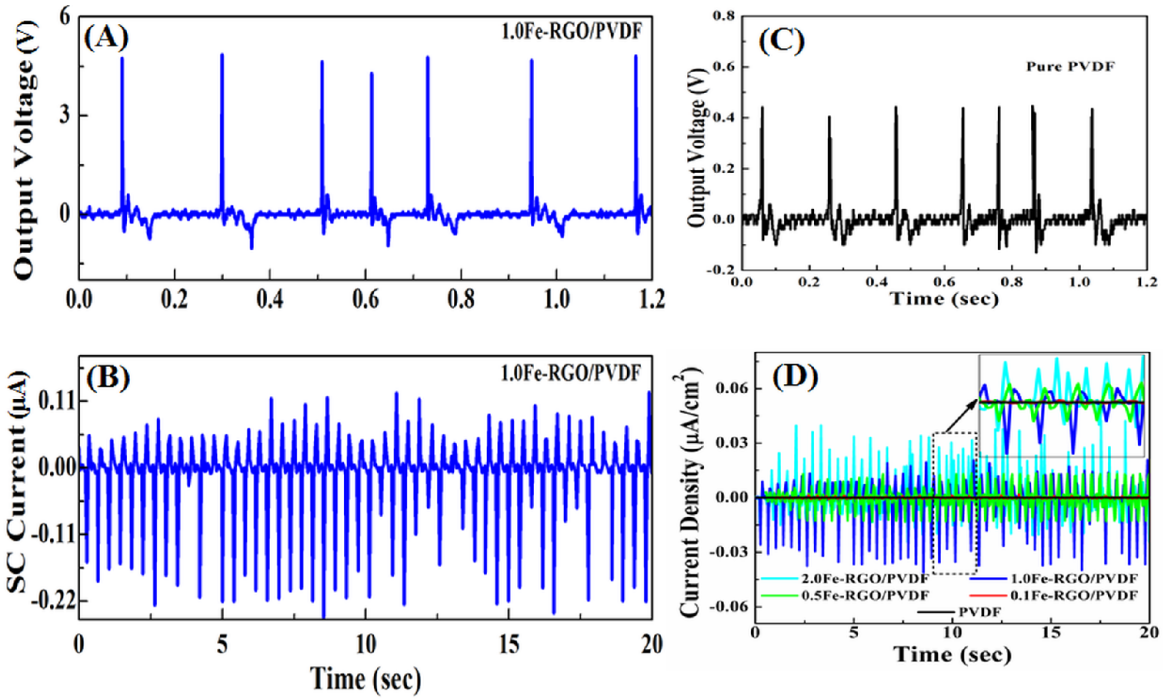

Fig. S13 (A) Output voltage and (B) short circuit (SC) current of 1.0Fe-RGO/PVDF nanocomposite film. (C) Output voltage of PVDF[14,15] and (D) current density of Fe-RGO/PVDF nanocomposite film at different Fe-RGO loading.

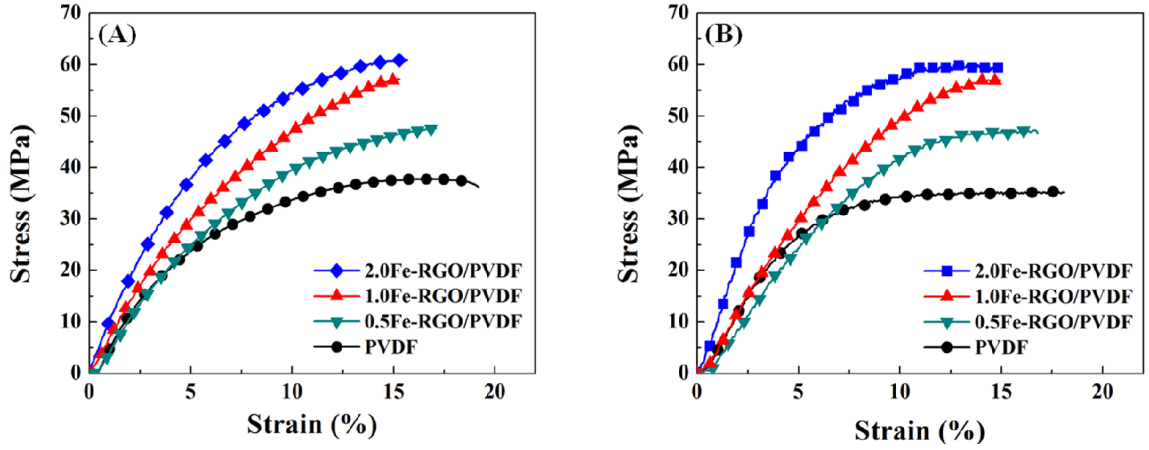

Fig. S14 Stress-strain behaviors of Fe-RGO/PVDF nanocomposite films at different Fe-RGO loading (A) before and (B) after (1500th times test) open circuit voltage and short circuit current measurement, respectively.

Table S1. The values of crystallinity of nanocomposite film at various filler loadings, obtained from XRD measurement.

Filler Loading	Percentage of crystallinity (χ_c)
0.0	42
0.1	43
0.5	44
1.0	46
2.0	48

Table S2. The DSC parameters and χ_c values of PVDDF and Fe-RGO/PVDF nanocomposite film at various filler loadings.

Filler loading	T_m (^{o}C)	T_c (^{o}C)	ΔH_m (J/g)	χ_c (%)
0.0	157.93	130.70	41.86	40
0.5	158.89	132.98	43.71	42
1.0	160.30	134.03	44.96	44
2.0	161.86	134.93	46.83	46

Table S3. The values of output pulse and maximum polarization of nanocomposite film at various filler loadings, obtained from ferroelectric measurement.

Fe-RGO (wt %)	Maximum Output Voltage (V)	Maximum polarization (P_{max}(μC/cm^2))
0.0	0.43	0.34

0.1	1.64	0.40
0.5	3.21	0.60
1.0	4.89	0.88
2.0	5.12	0.98

Table S4. The calculated values of released and loss energy density, efficiency of the nanocomposite at different filler loadings at an electric field of 537 kV/cm.

Fe-RGO (wt %)	Released energy density (U_R) (J/cm^3)	Energy loss density (U_L)(J/cm^3)	Efficiency ($U_R/(U_R+U_L)$)
0.0	0.27	0.17	0.60
0.1	0.32	0.20	0.61
0.5	0.49	0.31	0.62
1.0	0.73	0.48	0.60
2.0	0.85	0.49	0.63

Table S5. The maximum current density values of the Fe-RGO/PVDF nanocomposite films at different Fe-RGO loading.

Fe-RGO Loading	Maximum current density (J_{max} ($\mu A/cm^2$))
0.0	0.00000178
0.1	0.0084
0.5	0.0139
1.0	0.0409
2.0	0.0424

References

S1 W. Hummer and R. Offeman, *J. Am. Chem. Soc*., 1958, **80**, 1339–1340.

S2 Z. J. Fan, W. Kai, J. Yan, T. Wei, L. J. Zhi, J. Feng, Y. M. Ren, L.-P. Song and F. Wei, *ACS Nano*, 2011, **5**, 191–198.

S3 P. Martins, A. C. Lopes and S. L. Mendeza, *Prog. Polym. Sci*., 2014, **39**, 683–706.

S4 A. L. Morel, S. I. Nikitenko, K. Gionnet, A. Wattiaux and J. L. K. Him, *ACS Nano,* 2008, **2**, 847−856.

S5 X. Teng, D. Black, N. J. Watkins, Y. Gao, and H. Yang, *Nano Lett.*, 2003, **3**, 261−264.

S6 T. Yamashita, and P. Hayes, *App. Surf. Sci.*, 2008, **254**, 2441−2449.

S7 K. N. Kudin, B. Ozbas, H. C. Schniepp, R. K. Prudhomme, I. A. Aksay and R. Car, *Nano Lett.* 2007, **8**, 36−41.

S8 I. K. Moon, J. Lee, R. S. Ruoff and H. Lee, *Nat. Commun.*, 2010, **1**, 73.

S9 A. C. Ferrari and J. Robertson, *Phys. Rev. B*, 2000, **61**, 14095−14107.

S10 J. Zheng, H. Liu, B. Wu, Y. Guo, T. Wu, G. Yu, Y. Liu and D. Zhu, *Nano Res.*, 2011, **4**, 705–711.

S11 C. Pecharroman and J. S. Moya, *Adv Mater*., 2000, **12**, 294−297.

S12 K. Yu, H. Wang, Y. Zhou, Y. Bai and Y. Niu, *J. Appl. Phys*., 2013, **113**, 034105−034108.

S13 C. Hou, T. Huang, H. Wang, H. Yu, Q. Zhang and Y. Li, *Sci. Rep.*, 2013, 3, 1396.

S14 S. Garain, T. K. Sinha, P. Adhikary, K. Henkel, S. Sen, S. Ram, C. Sinha, D. Schmeißer and D. Mandal, *ACS Appl. Mater. Interfaces*, 2014, **7**, 1298–1307.

S15 R. A. Whiter, V. Narayan and S. Kar-Narayan, *Adv. Energy Mater.*, 2014, **4**, 1400519–1400525.